Journal of
Materials in Life Sciences

Vol. 3 No. 1 (2024)

Full Paper

Removal of Rhodamine 6G Dye using Pineapple Leaf Activated Carbon-Magnetite Sorbent

Yen Yee Lim[a], Nyuk Ting Ng[a] and Aemi Syazwani Abd Keyon[a,b]*

[a] Department of Chemistry, Faculty of Science, Universiti Teknologi Malaysia, 81310 UTM, Johor Bahru, Johor, Malaysia
[b] Centre for Sustainable Nanomaterials, Ibnu Sina Institute for Scientific and Industrial Research, Universiti Teknologi Malaysia, 81310 UTM Johor Bahru, Johor, Malaysia.

Article history
Received
26 March 2024
Revised
9 May 2024
Accepted
11 May 2024
Published online
30 May 2024

*Corresponding author
aemi@utm.my

Abstract

Pineapple leaf-activated carbon-magnetite (PLACM) was used as a sorbent for the removal of rhodamine 6G (R6G) dye from the aqueous phase. In this study, PLACM was characterized using Fourier transform infrared spectroscopy (FTIR), field emission scanning electron microscopy (FESEM), and *Brunauer-Emmett-Teller* (BET) techniques. FTIR spectra showed the presence of a Fe-O bond at 592 cm^{-1} in the PLACM, while FESEM analysis showed a rough, porous surface with some pores deposited by Fe_3O_4 particles. BET surface area for PLACM was 439.53 m^2/g. The removal efficiency of R6G dye was determined by UV-vis spectrophotometry and optimized using response surface methodology (RSM). Box-Behnken design (BBD) was employed to maximize R6G dye removal based on 17 experimental data. The parameters studied were the pH of the sample solution (pH 5-11), initial dye concentration (5-15 ppm) and sorbent dosage (6-14 mg). High correlation coefficients (R^2=0.9852) and low standard deviation (SD=1.47) confirmed the consistency of predicted values with respective experimental values and the adequacy of the quadratic model. The optimum conditions to remove R6G dye were pH 7.19, initial dye concentration of 10 ppm and 10 mg of PLACM. Good linearity was achieved with R^2=0.9853, while the limit of detection (LOD) and limit of quantification (LOQ) were 0.124 ppm and 0.376 ppm, respectively. Maximum removal of R6G dye in aqueous solution during optimization was 88.40%. As for real sample analysis, the removal percentage for R6G dye was 10.70±8.09%. Low adsorption ability was affected by the nature of the sorbent surface involved in the adsorption process. Negative charged PLACM surface site was applicable to positive charge basic dyes. However, disperse dyes used in the Uwin Textile Industry possess a negative charge in the solution, resulting in low removal performances due to the electrostatic repulsion between the negatively charged disperse dye and the negatively charged PLACM surface.

Keywords Rhodamine 6G, adsorption, activated carbon; pineapple leaf; magnetite

1.0 INTRODUCTION

According to World Bank research, textile dyeing and treatment account for 17-20% of industrial water contamination [1]. The most significant sources of this pollution come from various industries, such as textile, leather, food, cosmetic, paint/varnish, pharmaceutical, and pulp/paper industries. Dyes like methylene blue, rhodamine B, methyl orange, rhodamine 6G (R6G), methyl red, crystal violet, and others are commonly utilized in these industries. However, the presence of minute amounts of dyes in water (even less than 1 ppm) can impair the clearness of water, causing aesthetic issues due to the high visibility features of dyes [2]. Therefore, the amount of dissolved oxygen necessary to break down organic pollutants by microorganisms is studied

and referred to as biochemical oxygen demand (BOD, an indicator of the degree of organic pollution in water). When a high level of BOD is detected, it suggests the presence of oxygen deficiency due to significant organic pollution and intense microbial activity. The intense microbial activity results in higher oxygen demand and exceeds the normal replenishment rate, leading to an oxygen deficit in water. In coloured wastewater, BOD lowering (<50 ppm) is a harder task owing to the artificial origin of dyes with complex aromatic structures [3]. Moreover, dyes in aqueous environments reduce photosynthesis by preventing light penetration into the deeper layer of water, thus lowering the water quality. Therefore, decolorization of textile wastewater has long been a key environmental concern.

There are several approaches for treating dye effluents [4, 5]. Chemical approaches for treating wastewater containing dyes include coagulation-flocculation, photolysis, electrochemical and oxidation. Acid, direct, reactive, and vat dyes cannot be effectively decolored by coagulation-flocculation techniques. However, they can effectively decolorize some pigments, such as sulphur and dispersive dyes [5]. These techniques are often more expensive than physical and biological procedures. The limitations of these chemical approaches include high energy consumption, huge amounts of chemicals, and the need of adequate equipment. Furthermore, harmful by-products may be produced during the treatment process. Next, biological treatment is the employment of different biological organisms or technologies to remove contaminants from industrial effluent [6]. This technique aims to provide an efficient mechanism for disposing of breakdown products. Regarding wastewater purification, biological procedures outperform chemical and physical processes due to their ease of implementation, zero sludge, fewer chemical reagents needed, energy-saving features, and more eco-friendly and non-toxic by-products. However, the biological technique has a few drawbacks, including a long operation period and the inability of the biological organisms to function against harmful chemical substances. Wastewater generated by dyes can also be treated using various physical techniques, such as membrane filtration, irradiation, adsorption and ion exchange [7]. These physical techniques offer various advantages, such as simplicity of design, low cost, low chemical requirements, high flexibility, and ease of operation. While some of these procedures might not be ideal due to their limitations, like the generation of secondary sludge and partial application. Among these approaches, the adsorption process is one of the efficient and cost-effective ways to remove dyes, pigments, or colourants [9]. It is a process that transfers pollutants from one phase to another. Several sorbents, such as activated carbon [9-11], carbon [10], metal-organic framework [11], metal oxide [10], and polymer-based [14] sorbents, have been shown to remove dyes from wastewater effectively.

Because of their unique properties, these sorbents are employed to remove dyes from wastewater. Carbon-based materials such as graphene, carbon nanotubes and carbon nanofibers have tunable characteristics and high adsorption capacities, but they can be expensive to develop on a large scale. Metal-organic frameworks are porous materials of metal ions or clusters linked by organic ligands [13]. They often enable precise control over pore size and surface chemistry, but they can be difficult to synthesize and may have stability concerns in aqueous settings. Metal oxide-based sorbents, such as iron oxide (Fe_3O_4) or titanium dioxide (TiO_2), are long-lasting and interact strongly with pollutants. Still, they may have a weak affinity for certain organic adsorbates [10]. Polymer-based sorbents such as chitosan or polymeric resins are cost-effective, easy to regenerate, and can be modified for specific applications. However, modifying them for enhanced adsorption properties might be challenging due to their complex structure and composition. While activated, carbon is widely available, has a large surface area due to its high porosity, and is effective in adsorbing various pollutants, making it an excellent sorbent for dye [16-17]. Therefore, activated carbon is the most commonly used sorbent for dye removal through adsorption [1, 15]]. Activated carbon can be produced from natural resources or agricultural solid waste [16, 18], which is more cost-effective. This is due to the fact that agricultural solid waste generated by agricultural operations is readily available. Examples of the natural resources for the making of activated carbon include coconut shell [9, activated corn leaf carbon [20], lemongrass leaf [21], citrus sinensis leaf [22], cattail biomass [23], Palmyra (palm) shell [24], etc. Pineapple leaf can also be used as a raw material for sorbent due to its high fibre content, which can form more porous structures. Moreover, pineapple leaf is an abundant agricultural waste product in Malaysia, making them a sustainable and environmentally beneficial supply of activated carbon. Therefore, these inexpensive and abundant raw materials have the potential to produce activated carbon with a large surface area [25], which contributes to high adsorption capacity. In this study, pineapple leaf-activated carbon-magnetite (PLACM) was developed as a sorbent for the removal of R6G dye. The sorbent was magnetized to simplify the sorbent separation process with external magnetic strength. Box-Behnken design (BBD), one of the common experiment design tools used in response surface methodology (RSM), was also adopted in this study to optimize the R6G removal process. After validating the adsorption process, PLACM was applied to remove R6G in real textile wastewater.

2.0 EXPERIMENTAL

2.1 Materials

All reagents were analytical reagent grade and used without further purification. Ferrous sulphate heptahydrate ($FeSO_4.7H_2O$, 99.5%), ferric chloride hexahydrate ($FeCl_3$.6H2O, 99.5%), orthophosphoric acid (H_3PO_4, 85.0%), sodium hydroxide pellet (NaOH, 99.5%), ethanol (C_2H_5OH, 99.8%), and hydrochloric acid (HCl) were acquired from QReC (Shah Alam, Selangor,

Malaysia). Deionized water (DI) was obtained from the Millipore water purification system (Molsheim, France). Dye standard R6G was purchased from BDH Chemicals Ltd Poole (England). Pineapple leaves are purchased from local markets. A series of standard solutions ranging from 5 to 15 ppm were prepared by dilution from stock solution for instrumental calibration purposes.

2.2 Preparation of materials

2.2.1 Preparation of pineapple leaf activated carbon (PLAC)

The PLAC had been previously synthesized in-house in accordance with the method developed by Kamarulzaman [26]. At first, 30 g of pineapple leaf was immersed in 150 ml of 55% w/w acid (H_3PO_4) to pretreat the leaf. After that, excess acid was removed from the material and dried overnight at 104ºC. The material was calcined at 550ºC for 2hr, producing black activated carbon. Then, the material was centrifuged at 4000 rpm for 10 min and rinsed several times until the pH reached neutral. The final product was then dried for 2 hr in an oven at 110ºC. The PLAC product was ground to a fine powder and stored in a desiccator before usage.

2.2.2 Synthesis of pineapple leaf activated carbon magnetite (PLACM)

The PLACM was previously synthesized in-house using the method developed by Kamarulzaman [26]. 1.38 g of $FeCl_3$ and 0.70 g of Fe_SO_4 were mixed into 100 mL of distilled water. Then, 0.5 g of PLAC was added to the solution and agitated for 15min. After that, the solution was agitated again at 60°C for 2 hr. The pH was then adjusted by adding 10 M NaOH dropwise until it reached pH 10, and the mixture was agitated constantly for another 2hr. The presence of black precipitate indicated the occurrence of a co-precipitation process. Following that, the solution was kept at room temperature for 24 hr. To establish a neutral pH, magnetite particles were repeatedly washed with deionized water and ethanol. Lastly, the product was dried at 80ºC for 24 hr and stored in a desiccator before use.

2.3 Characterization of Materials

The instrument used to study R6G dye was Shimadzu UV-visible spectrophotometer (UV-1800) (Petaling Jaya, Selangor, Malaysia). For sorbent characterization, Perkin Elmer TM400 Fourier Transform Infrared Spectrophotometer (FTIR) (Waltham, USA) was employed for functional group study in the range of 4000-400cm^{-1}. JEOL-6710 Field Emission Scanning Electron Microscopy (FESEM) (Tokyo, Japan) was used for morphology analysis. The *Brunauer-Emmett-Teller* (BET) surface area analysis was performed to determine the sorbent's surface information with Elementar Analyzer Vario Micro Cube (Germany). The vortex mixer from Velp Scientifica (Shah Alam, Selangor, Malaysia) was employed for the complete sorbent dispersion in the aqueous phase. pH meter (pH 700) obtained from Eutech Instrument Pte Ltd (Ayer Rajah Crescent, Singapore) was used to adjust the solution pH. Microwave oven from Memmert (Schwabach, Bavaria, Germany) and furnace box from Ney Vulcane 3-550 (Yucaipa, California, USA) were employed in this study for heating or drying purposes. Ohaus analytical balance (Singapore) was employed for mass measurement. Software DX7 Design Expert 7 (Stat-Ease Inc, United States) was used for the optimization study using the BBD method.

2.4 Removal study

All the experiments were conducted according to the BBD matrix. Minimum and maximum values of the three optimization parameters (solution pH, initial dye concentration and sorbent dosage) were determined from pre-trail experiments. 10 mg of PLACM was added into 10 mL of sample solution of dyes with an initial concentration of 10 ppm. After that, the solution pH was adjusted to pH 8 by adding 0.1 M of HCl or NaOH. The mixture was shaken for 5 min. Then, an external magnetic field separated the sample and the aqueous phase. UV-vis analysis for R6G was carried out to study the efficiency of the sorbent.

2.5 PLACM surface charge study

Six Erlenmeyer flasks (250 mL) containing 40 mL of 0.1 M KNO_3 salt solution were prepared. These solutions were adjusted to pH 1, pH 2, pH 4, pH 6, pH 8, and 10 as pH_i by using 0.1 M to 1.0 M of NaOH and HNO_3. 100 mg of PLACM was added to each flask and shaken at maximum speed at room temperature for 24 hr. Then, the final pH (pH_f) of each solution was measured. Difference between pH_i and pH_f (ΔpH) against pH_i was plotted.

2.6 Optimization study

Experimental design, response surface modelling and process optimization were included in this study. Three parameters, which are solution pH, initial dye concentration and sorbent dosage, are labelled as X_1, X_2 and X_3, respectively. Each variable consisted of 3 levels: a low, middle, and high level, which were designated as -1, 0, and +1, respectively. Mathematical relationships between response and variables were calculated by developing a polynomial equation. The accuracy and reliability of the model were analyzed using coefficients obtained through the application of ANOVA and multiple regression analysis. To optimize the removal experiment, parameters included solution pH (5-11), initial dye concentration (5-15 ppm) and dosage of sorbent (6-14 mg) were evaluated. A total of 17 experiments were performed to estimate the coefficient.

3.0 RESULTS AND DISCUSSION

3.1 Characterization of PLACM sorbent

PLACM was characterized using FTIR, FESEM, and BET analysis to determine its functional groups, morphology, and specific surface area. The point of zero charge, pH_{pzc}, was studied to understand the charge of the sorbent surface under different pH conditions.

3.1.1 FTIR study

Figure 1 (i) a, b and c shows FTIR spectra for PLAC, Fe_3O_4, and PLACM, respectively. From these three spectra, 3437, 3437 and 3431 cm^{-1} peaks are assigned to OH stretching. C-H stretching is evident in PLAC and PLACM, with adsorption bands at 2920 and 2924 cm^{-1}. Next, OH bending in PLAC, Fe_3O_4, and PLACM due to adsorbed water molecules has corresponding adsorption peaks at 1627, 1634, and 1629 cm^{-1}, while 633 and 583 cm^{-1} in Fe_3O_4 are assigned to Fe-O bonds. The adsorption peak at 592 cm^{-1} in PLACM is ascribed to the Fe-O bond, indicating that a magnetic composite was successfully synthesized [27]. However, the absence of the Fe-O bond in PLAC was determined as there is no spectrum below 600 cm^{-1}.

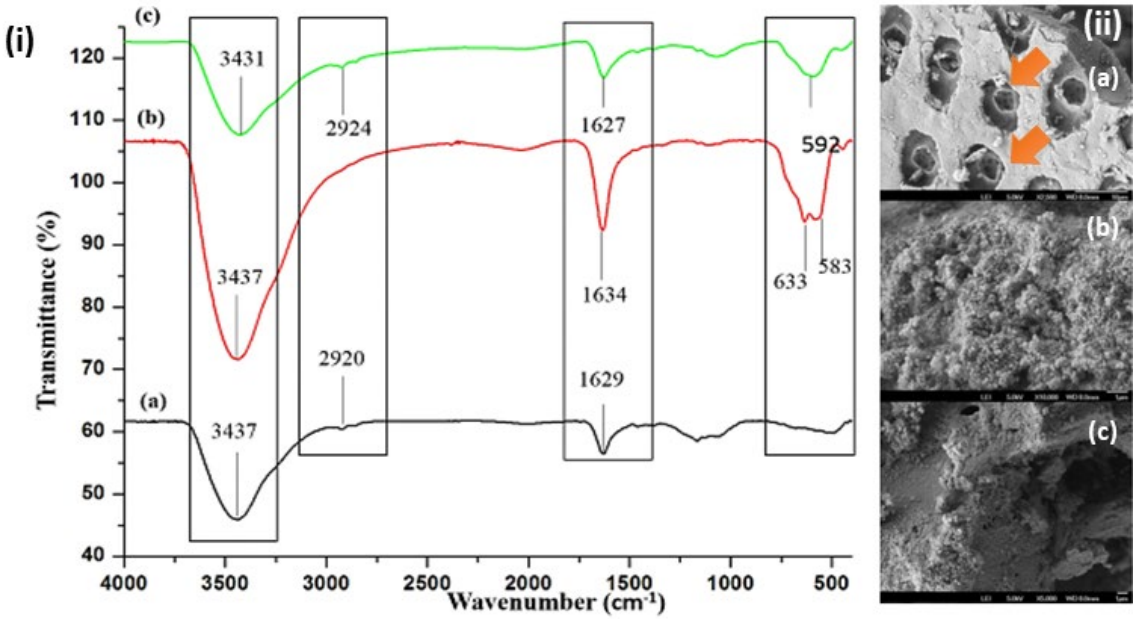

Figure 1 (i) FTIR spectra of (a) PLAC (b) Fe_3O_4 and (c) PLACM; (ii) FESEM images of (a) PLAC (b) Fe_3O_4 and (c) PLACM.

3.1.2 FESEM study

Figure 1 (ii) (a) depicts PLAC at a magnification of 2,500×. Porous structures on the sorbent surface were observed due to phosphoric acid's activation process. This is because phosphoric acid is an effective activating agent, triggering chemical events with the carbon precursor. It reacts with carbonaceous material during activation, causing gasification and chemical etching. Eventually, these processes result in the formation of pores inside the material's structure. Also, an uneven distribution of

activation agents occurred during the activation process, resulting in variances in pore creation across the material's surface. Furthermore, impurities or non-carbonaceous components in the precursor material may contribute to the formation of non-porous residues or surface coatings, preventing pore development in specific places. Ash was observed on the surface of the sorbent, as evident by the white spot on the image. Figure 1 (ii) (b) shows the surface morphology of Fe_3O_4 at a magnification of 10,000×. The spherical form particles are found aggregated due to the magnetic dipole attraction [28]. In Figure 1 (ii) (c), PLACM at 5,000× magnification was observed, with some pores being covered. The particles covering the pores are most likely Fe_3O_4 particles. This could be due to the co-precipitation reaction between PLAC and an iron salt combination containing $FeCl_3$ and $FeSO_4$.

3.1.3 BET study

The BET report of PLACM showed that its specific surface area and pore volume were 439.53 m^2/g and 0.5717 cm^3/g, respectively. It can be concluded that PLACM had both micro- and mesoporous properties, with the average radius of pores of 5.311 nm and the size ranging from 0.31 to 1.0 nm. A bigger surface area of PLACM could provide more active adsorption sites. At the same time, a larger pore volume may allow the R6G molecules easier access to these locations, contributing to its high adsorption performance for R6G.

3.1.4 Surface charge study PLACM

The pH of PLACM at neutral conditions is known as pH_{PZC}. pH_{PZC} is identified from the x-intercept of the graph that plots the ΔpH against pH_i. Based on the graph, pH_{PZC} is pH 7.2. The sorbent surface acquires positive surface charges at solution pH levels lower than pH_{PZC}. In contrast, negative surface charges appear on the sorbent surface when the solution pH exceeds pH_{PZC}. When sorbent surfaces become protonated at acidic conditions, electrostatic repulsion arises between the positive surface charge and the basic R6G dye in the presence of bulk H^+ ions. This reduced the sorbent's adsorption capabilities in acidic conditions. The adsorption of R6G dye on PLACM is preferred at alkaline conditions due to the electrostatic attraction between the negative charge surface and the positive charge. Although electrostatic repulsion persists, physisorption continues due to weak Van der Waal forces between the R6G dye and the sorbent surface.

3.2 Response surface modelling

The process variables were optimized using BBD, an RSM optimization tool. RSM is better suited for optimization than traditional single-variable optimization, as it can save more time, space, and raw materials. Table 1 lists the three parameters in this study that were optimized using RSM.

Table 1 Process control variables and their limits.

Variable	Unit	Notation	Limit		
			-1	0	+1
pH	-	pH	5	8	11
Initial concentration	mg/L	C_0	5	10	15
Dosage of sorbent	mg	D	6	10	14

The optimization method was carried out using the BBD matrix. Table 2 presents the experimental data and results. Two removal tests were performed per run, with the average removal percentages recorded. RSD less than 10% indicates great precision. The analysis of variance (ANOVA) tables was generated to determine the significance of linear term (A, B, C), quadratic (A^2, B^2, C^2) and the interaction term (AB, AC and BC) for regression coefficient. The best fit of the model is shown in equation 1:

$$Y=84.99 - 6.54X_1 - 3.91X_2 + 4.19X_3 – 1.98X_1X_2 - 3.14X_1X_3 + 2.00X_2X_3 -7.95X_1^2 - 0.84X_2^2 – 3.33X_3^2 \quad \text{(Equation 1)}$$

where Y refers to adsorption ability, X_1, X_2, and X_3 are pH, initial concentration for dye solution and dosage of sorbent, respectively. The accuracy and significance of the model can be further estimated by using the ANOVA method as well. From

Table 3, this model was significant with a large F value (F_{model} = 51.83) and low p-value (p_{model} <0.0001). There was only a 0.01% chance that this large F_{model} value could occur due to noise. Lack of fit measures the model's failure to represent data in the experimental domain at points not included in the regression [29]. Besides, it can be used to determine how the proposed model fits well with experimental data and the effect of each variable on the response. P value (<0.05) confirms that the quadratic model is statistically significant for response and, therefore, can explain the actual relationship between response and significant variables [29]. F and P values of lack of fits for this model were 5.93 and 0.0592, respectively. This implies that lack of fit is not significant relative to the pure error, and the model represents the relationships of variables well within the ranges selected. Therefore, the experimental result was best fitted with Equation 1. It was known that the smaller the P-value and the larger the degree of the F-value, the more significant the corresponding coefficient is [31]. From F-value, a variable that brings the most significant effect is pH. Besides, model terms A, B, C, AB, AC, BC, A_2, C_2 were significant because the P-values were less than 0.0500.

Table 2 BBD matrix.

Run	pH	C_0	D	Removed percentage 1 (%)	Removed percentage 2 (%)	Average percentage (%)	SD	RSD (%)
2	5	5	10	85.30	85.75	85.53	0.32	0.37
15	11	5	10	77.20	76.43	76.82	0.54	0.71
12	8	5	6	81.99	82.17	82.08	0.13	0.16
16	8	5	14	86.43	84.07	85.25	1.67	1.96
10	5	10	6	73.24	71.77	72.51	1.04	1.43
1	11	10	6	63.50	67.12	65.31	2.56	3.92
5	5	10	14	87.91	88.89	88.40	0.69	0.78
14	11	10	14	67.30	69.96	68.63	1.88	2.74
8	8	10	10	85.14	85.43	85.29	0.21	0.24
17	8	10	10	83.55	86.52	85.04	2.10	2.47
4	8	10	10	84.85	83.97	84.41	0.62	0.74
7	8	10	10	84.34	83.47	83.91	0.62	0.73
9	8	10	10	84.93	85.64	85.29	0.50	0.59
6	5	15	10	80.86	78.24	79.55	1.85	2.33
3	11	15	10	61.30	64.52	62.91	2.28	3.62
13	8	15	6	70.30	74.5	72.40	2.97	4.10
11	8	15	14	82.18	84.94	83.56	1.95	2.34

* SD=standard deviation; RSD=relative standard deviation

Table 3 ANOVA table for response surface quadratic model.

Source	Sum of Squares	df	Mean Square	F Value	p-value Prob > F

Model	1010.41	9	112.27	51.83	< 0.0001	Significant
A-pH	342.17	1	342.17	157.95	< 0.0001	
B-initial concentration	122.15	1	122.15	56.39	0.0001	
C-dosage	140.62	1	140.62	64.91	< 0.0001	
AB	15.72	1	15.72	7.26	0.0309	
AC	39.50	1	39.50	18.23	0.0037	
BC	15.96	1	15.96	7.37	0.0300	
A^2	265.97	1	265.97	122.78	< 0.0001	
B^2	2.96	1	2.96	1.36	0.2811	
C^2	46.63	1	46.63	21.52	0.0024	
Residual	15.16	7	2.17			
Lack of Fit	12.38	3	4.13	5.93	0.0592	Not significant
Pure Error	2.79	4	0.70			
Cor Total	1025.58	16				

In addition, the normal distribution or normality of residuals of a model could be verified by a normal probability plot of the residuals. Normal distribution could be proved with the regression data fitted almost near a straight line on the graph and approximately linear (Figure 2 (i)). A plot of predicted versus actual values of the experiment is shown in Figure 2 (ii). The consistency of predicted values with respective experimental values could be confirmed with high correlation coefficients (R^2=0.9852) and low standard deviation (SD=1.47). This indicates the adequacy of the fitted quadratic model for predictive applications [32]. R^2 indicates how perfect the model is for estimating experimental data, while adjusted R^2 determines the amount of variation in the mean by model. R_{adj}^2 =0.9662 suggests that the total variation of 96% for percentage removal to independent variables and only an approximation of 4% of the total variation cannot be explained by the model. Moreover, high adjusted correlation coefficient values (R_{adj}^2 =0.9662) close to 1 indicate high reliability in predicting the experimental data [33]. The signal-to-noise ratio consists of the predicted value at the design point and the average prediction error. "Adeq Precision" that measured the signal-to-noise ratio was desirable with a ratio greater than 4. In this study, the ratio of 21.097 indicated an adequate signal [33].

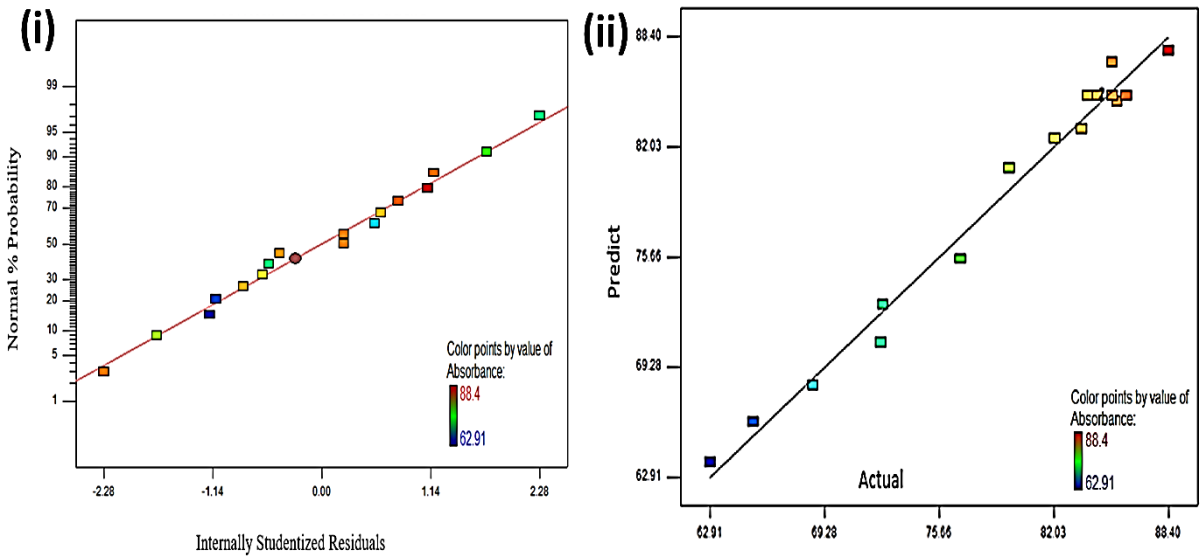

Figure 2 (i) Normal plot of residuals; (ii) Plot of predicted versus actual values.

3.3 Effect of process variables

The interaction of process variables significantly affects removal percentages. The effects of process variables on pH and the initial concentration of dyes (AB), pH and the dosage of sorbent (AC), and the initial concentration of dyes with the dosage of sorbent (BC) were studied from their respective 3D surface and contour plots.

3.3.1 Effect of pH and initial concentration of dye

The interactive effect of solution pH and initial concentration of dye on the adsorption by PLACM is shown in Figure 3 (a). The removal percentage depended on the solution pH as its linear and quadratic effects were significant ($p< 0.05$). Hence, the graph showed a curvilinear nature. pH is one of the important factors as pH can affect the degree of ionization of dye. The percentage removal of R6G dye decreased with increased pH. At 15 ppm dye concentration, percentage removal decreased from 84.56% to 67.93%, while at 5 ppm, percentage removal decreased from 85.53% to 76.52%. Theoretically, adsorption of positive charge R6G dye is favourable under alkali conditions as PLACM has pH_{PZC}=7.2. A positive surface charge of PLACM exists under solution pH 7.2. Electrostatic repulsion exists between R6G dye and sorbent at low solution pH. In this study, the removal percentage increased at low solution pH and decreased after pH 8. Dye adsorption on PLACM was not favourable under alkaline conditions [34]. This is due to the attraction of the negative charge cloud towards the positive charge PLACM surface. The negative charge cloud is formed by delocalizing “π” electrons in the aromatic ring [34].

Initial dye concentration was another factor contributing to the percentage of removal with its significant linear, interaction term and an insignificant quadratic term. Thus, there was a linear decrease in removal percentage with an increase in initial dye concentration for all pH. At solution pH 5, percentage removal decreased from 85.53% to 79.55%; at solution pH 11, it decreased from 76.82% to 62.91%. This is due to the limited active site on the sorbent surface, which is not applicable for all adsorbates in bulk solution to be adsorbed onto the sorbent surface. At constant dosage of sorbent, low percentage removal of R6G is due to less availability of adsorption site of sorbent at higher initial dye concentration [36]. The highest removal of R6G dye (86.04%) was achieved under the conditions: solution pH 8, 10 ppm of initial concentration and constant of 10 mg sorbent.

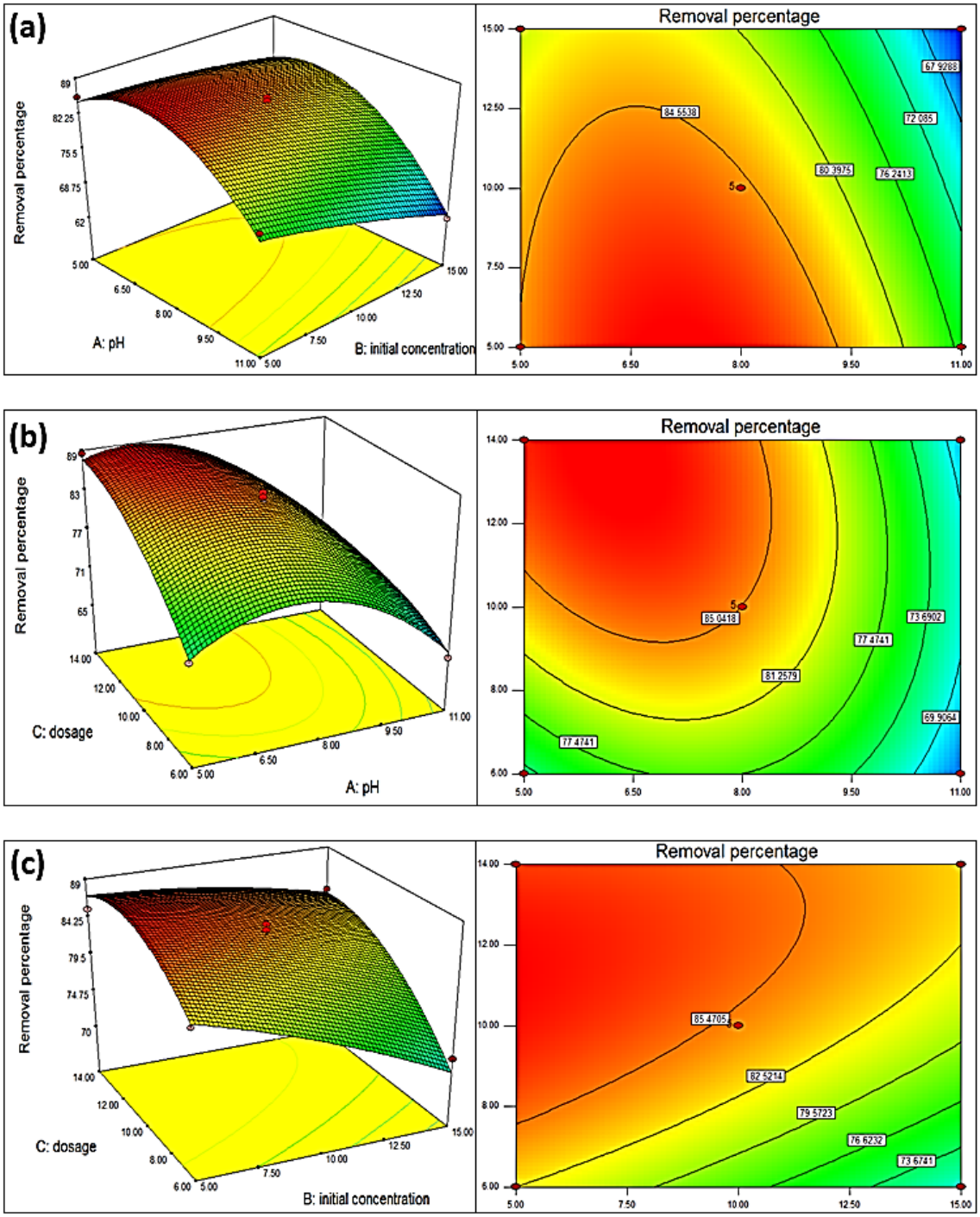

Figure 3 3D surface plot and Contour plot based on the effect of (a) pH and initial concentration of dye; (b) pH and dosage of sorbent; (c) initial concentration of dye and dosage of sorbent.

3.3.2 Effect of pH and dosage of sorbent

Figure 3 (b) shows the combined effect of pH and dosage for sorbent. pH and sorbent dosage were important factors as a linear term, quadratic term, and interaction term were significant for both factors. The percentage removal for R6G increased at lower solution pH and decreased after pH 8. Percentage removal decreased from 72.51% to 65.31% when 6 mg of PLACM was used in adsorption. When 14 mg of PLACM was used, percentage removal decreased from 88.40% to 68.63%. There was a decrease in percentage removal with 14 mg compared to 6 mg of PLACM. Solution pH only slightly influenced adsorption when the low dosage of sorbent was used. This is because R6G from bulk solution can still adsorb onto the limited active sites on the surface through physisorption and without considering the ionization degree of R6G.

In addition, the removal percentage of dye increased with increasing sorbent dosage. Linear rising (72.51% to 88.40%) and slowly rising (65.31% to 68.63%) removal percentages were observed at low and high pH, respectively. This is because the adsorption of R6G dye onto PLACM was favourable under low pH or slightly acidic conditions. As pH 5 is higher than Rh6G's pKa (about 2.34), most Rh6G molecules are likely deprotonated. Rh6G is negatively charged when deprotonated. While the adsorbent exhibits a positive surface charge and interacts electrostatically with the R6G at pH 5 [37]. More adsorbate can also adsorb on high dosages of PLACM due to additional active sites compared to low dosages under low pH. The Linear increase in removal percentage at low pH was due to a significant difference in the amount of adsorbate absorbed onto the surface. Therefore, the highest removal percentage for R6G dye (88.04 %) was determined at pH 5 and 14 mg sorbent, while 10 ppm of dye solution was kept constant.

3.3.3 Effect of initial concentration of dye and dosage of sorbent

The response surface plot for the interactive effect of the initial concentration of dye and dosage of sorbent is shown in Figure 3 (c). There was a slight increase in removal percentage (83.56% to 85.25%), with a decrease in initial concentration observed in high sorbent dosage. This is due to a large number of active sites on the sorbent surface with increasing dosage. Almost all the adsorbate in bulk solution is being adsorbed onto the surface. Similarly, Gecgel et al. [38] also reported that the initial dye concentration does not bring significant changes in the dye removal percentage.

Besides, the removal percentage increased linearly with a dosage of sorbent, where 82.08% increased to 83.56% at 5 ppm and 72.40% increased to 83.56% at 15 ppm. This is due to the number of active sites on the sorbent surface that is directly proportional to the sorbent dosage. Maximum removal of R6G dye (85.29%) was determined at 10 ppm of dye solution, 10 mg sorbent and at constant pH 8. The graph showed a curvilinear nature as linear and quadratic terms for dosage are significant ($p<0.05$).

3.4 Method validation

Method calibration graph for R6G dye solution in the concentration range from 3.4 pm to 9.4 ppm was performed. Fixed conditions employed throughout the adsorption experiment were solution pH 7.19, 10 mg of sorbent, and 5 min of stirring time. The optimum condition from RSM was solution pH 7.19, 5.40 ppm of initial concentration for dye solution, and 10 mg of sorbent. The coefficient of determination (R2) was 0.9853, while the limit of detection (LOD) and limit of quantification (LOQ) were calculated as 0.124 ppm and 0.376 ppm, respectively. The calculated linear index for this graph (x'/x) was from 0.97 to 1.20. Precisions of the experiment were performed and expressed by repeatability (intra-day precision) and reproducibility (inter-day precision). The experiments were precise, with an RSD of less than 10%, as shown in Table 4.

Table 4 Repeatability and reproducibility of adsorption experiment on optimum conditions: solution pH 7.19, 5.4 ppm of initial concentration and 10 mg sorbent.

Precisions	Removal percentage for triplicate (%)	Average removal percentage (%)	SD	RSD (%)
Repeatability Day 1	82.95 82.19 80.57	81.90	1.22	1.48
Repeatability Day 2	84.69 87.08 86.79	86.19	1.30	1.51
Repeatability Day 3	83.96 84.33 84.80	84.36	0.42	0.50
Reproducibility (n = 9)	82.95 82.19 80.57 84.69 87.08 85.27 83.96 84.33 84.80	83.98	1.89	2.25

* SD=standard deviation; RSD=relative standard deviation

3.5 Removal of dyes in real wastewater

PLACM was used to remove R6G dye from dye effluent. The real dye wastewater was from Uwin Textile Industries, Larkin Industrial Estate, Johor Bahru. Prior to analysis, the sample was filtered first using filter paper, and 50 ml of the sample was spiked with R6G dye standard solution to reduce the matrix effect in the wastewater sample. The initial and final absorbance of the sample was analyzed using a UV-vis spectrophotometer to determine removal efficiency.

Based on the matrix-matched calibration graph, the coefficient of determination (R^2) was 0.9892, while LOD and LOQ were calculated as 0.026 ppm and 0.079 ppm, respectively. The calculated linear index for this graph was from 0.96 to 1.12. However, the removal percentage for dye wastewater was low, 10.70 ± 8.09%. This might be due to the nature of the sorbent surface involved in the adsorption process, which is one of the major factors in determining the adsorption performance. PLACM has a negatively charged surface site, which applies to basic dyes with a positive charge. However, the main dye ingredient of the wastewater obtained from the Uwin Textile industry was disperse dye. Disperse dye is a non-ionic dye that often possesses a negative charge in solution. Therefore, electrostatic repulsion might occur between the dispersed dye and sorbent, resulting in poor removal percentages. Also, these dyes always form colloids in solution due to low solubility in water. The colloidal nature and low solubility of dispersed dyes could lead to poor adsorption of dyes on carbon [39].

4.0 CONCLUSION

PLACM had been utilized as a sorbent in removing R6G dye due to its high surface area and adsorption capacity. Techniques like FTIR, FESEM and BET were performed to characterize PLACM. These characterization results indicate that the PLACM was synthesized successfully. BBD was employed to study the optimization removal of R6G dye, with pH (5-11), initial dye concentration (5-15 ppm) and dosage of sorbents (6-14 mg) as the studied variables. The optimum conditions for removal of R6G dye were pH 7.19, initial dye concentration of 10 ppm and 10 mg of PLACM. These optimized data were further validated by a standard calibration curve of R6G dye, with R^2 =0.9896, LOD of 0.124 ppm and LOQ of 0.376 ppm. The precision of experiments was validated through repeatability study with removal percentages of 81.90% ± 1.48 (day 1), 85.68% ± 1.45 (day 2), 84.36% ± 0.50 (day 3), and reproducibility with 83.98% ± 2.25. The concentration of R6G in real industrial wastewater was found to be 0.8 ppm. LOD and LOQ for industrial wastewater analysis were determined as 0.026 ppm and 0.079 ppm, respectively.

Acknowledgment

A.S.A.K would like to acknowledge Kurita Water and Environment Foundation (KWEF) for the Kurita Asia Research Grant (grant number: 23Pmy005, cost centre number: R.J130000.7354.1U025, reference number: PY/2023/02919) awarded for this work.

References

[1] Rafiq, A., Ikram, M., Ali, S., Niaz, F., Khan, M., Khan, Q., and Maqbool, M. 2021. Photocatalytic degradation of dyes using semiconductor photocatalysts to clean industrial water pollution. Journal of Industrial and Engineering Chemistry. 97: 111-128.

[2] Alsukaibi, A. K. 2022. Various approaches for the detoxification of toxic dyes in wastewater. Processes. 10(10): 1968.

[3] Pai, S., Kini M. S., and Selvaraj R. 2021. A review on adsorptive removal of dyes from wastewater by hydroxyapatite nanocomposites. Environmental Science and Pollution Research. 28(10): 11835-11849.

[4] Hanafi, M. F. and N. Sapawe. 2020. A review on the current techniques and technologies of organic pollutants removal from water/wastewater. Materials Today: Proceedings. 31: A158-A165.

[5] Solayman, H. M., Hossen, M. A., Abd Aziz, A., Yahya, N. Y., Leong, K. H., Sim, L. C., Monir, M. U. and Zoh, K. D. 2023. Performance evaluation of dye wastewater treatment technologies: A review. Journal of Environmental Chemical Engineering. 11(3): 109610.

[6] Shabir, M., Yasin, M., Hussain, M., Shafiq, I., Akhter, P., Nizami, A. S., Jeon, B. H. and Park, Y. K. 2022. A review on recent advances in the treatment of dye-polluted wastewater. Journal of Industrial and Engineering Chemistry. 112: 1-19.

[7] Roy, M. and R. Saha. 2021. Dyes and their removal technologies from wastewater: A critical review, in Intelligent Environmental Data Monitoring for Pollution Management, Bhattacharyya, S., Mondal, N. K., Platos, J., Snášel, V., Krömer, P., Editors. Academic Press. 127-160.

[8] Dutta, S., Gupta, B., Srivastava, S. K. and Gupta, A. K. 2021. Recent advances on the removal of dyes from wastewater using various adsorbents: A critical review. Materials Advances. 2(14): 4497-4531.

[9] Parida, V. K., Srivastava, S. K., Gupta, A. K., and Rawat, A. (2023). A review on nanomaterial-based heterogeneous photocatalysts for removal of contaminants from water. Materials Express. 13(1): 1-38.

[10] Moosavi, S., Lai, C. W., Gan, S., Zamiri, G., Akbarzadeh Pivehzhani, O. and Johan, M. R. 2020. Application of efficient magnetic particles and activated carbon for dye removal from wastewater. ACS omega. 5(33): 20684-20697.

[11] Sultana, M., Rownok, M. H., Sabrin, M., Rahaman, M. H. and Alam, S. M. N. 2022. A review on experimental chemically modified activated carbon to enhance dye and heavy metals adsorption. Cleaner Engineering and Technology. 6: 100382.

[12] Sabzehmeidani, M. M., Mahnaee, S., Ghaedi, M., Heidari, H. and Roy, V. A. 2021. Carbon based materials: A review of adsorbents for inorganic and organic compounds. Materials Advances. 2(2): 598-627.

[13] Parmar, B., Bisht, K. K., Rajput, G. and Suresh, E. 2021. Recent advances in metal–organic frameworks as adsorbent materials for hazardous dye molecules. Dalton Transactions. 50(9): 3083-3108.

[14] Mok, C. F., Ching, Y. C., Muhamad, F., Abu Osman, N. A., Hai, N. D. and Che Hassan, C. R. 2020. Adsorption of dyes using poly(vinyl alcohol) (PVA) and PVA-based polymer composite adsorbents: A review. Journal of Polymers and the Environment. 28: 775-793.

[15] Azam, K., Shezad, N., Shafiq, I., Akhter, P., Akhtar, F., Jamil, F., Shafique, S., Park, Y.-K. and Hussain, M. 2022 A review on activated carbon modifications for the treatment of wastewater containing anionic dyes. Chemosphere. 306: 135566.

[16] Nizam, N. U. M., Hanafiah, M. M., Mahmoudi, E., Halim, A. A. & Mohammad, A. W. 2021. The removal of anionic and cationic dyes from an aqueous solution using biomass-based activated carbon. Scientific Reports. 11(1): 1-17.

[17] Jawad, A. H., Abdulhameed, A. S., Wilson, L. D., Syed-Hassan, S. S. A., Alothman, Z. A. and Khan, M. R. 2021 High surface area and mesoporous activated carbon from KOH-activated dragon fruit peels for methylene blue dye adsorption: optimization and mechanism study. Chinese Journal of Chemical Engineering. 32: 281-290.

[18] Paul Nayagam, J.O. and K. Prasanna. 2022. Utilization of shell-based agricultural waste adsorbents for removing dyes: A review. Chemosphere. 291: 132737.

[19] Widiyastuti, W., Rois, M. F., Suari, N. M. I. P. & Setyawan, H. 2020. Activated carbon nanofibers derived from coconut shell charcoal for dye removal application. Advanced Powder Technology. 31(8): 3267-3273.

[20] Sunkar, S., Prakash, P., Dhandapani, B., Baigenzhenov, O., Kumar, J. A., Nachiyaar, V., Zolfaghari, S., Sara, Tejaswini and Hosseini-Bandegharaei, A. 2023. Adsorptive removal of acid blue dye 113 using three agricultural waste biomasses: The possibility of valorization by activation and carbonization – A comparative analysis. Environmental Research. 233: 116486.

[21] Ahmad, M. A., Ahmed, N. A. B., Adegoke, K. A. and Bello, O. S. 2021. Adsorptive potentials of lemongrass leaf for methylene blue dye removal. Chemical Data Collections. 31: 100578.

[22] Messaoudi, N. E., Mouden, A. E., Khomri, M. E., Bouich, A., Fernine, Y., Ciğeroğlu, Z., Américo-Pinheiro, J. H. P., Labjar, N., Jada, A., Sillanpää, M. and Lacherai, A. 2023. Experimental study and theoretical statistical modeling of acid blue 25 remediation using activated carbon from Citrus sinensis leaf. Fluid Phase Equilibria. 563: 113585.

[23] Yu, M., Han, Y., Li, J. and Wang, L. 2017. CO_2-activated porous carbon derived from cattail biomass for removal of malachite green dye and application as supercapacitors. Chemical Engineering Journal. 317: 493-502.

[24] Muniyandi, M. and Govindaraj, P. 2021. Potential removal of Methylene Blue dye from synthetic textile effluent using activated carbon derived from Palmyra (Palm) shell. Materials Today: Proceedings. 47: 299-311.

[25] Rosli, N. A., Ahmad, M. A., Noh, T. U. and Ahmad, N. A. 2023 Pineapple peel–derived carbon for adsorptive removal of dyes. Materials Chemistry and Physics. 306: 128094.

[26] Kamarulzaman, F. F. B. 2018. Pineapple leaf activated carbon-magnetite as an adsorbent for magnetic solid phase extraction of heavy metals in liquid detergent samples. Bsc Thesis, Universiti Teknologi Malaysia, Skudai. 18-19.

[27] Hong, R. Y., Li, J. H., Li, H. Z., Ding, J., Zheng, Y. & Wei, D. G. 2008. Synthesis of Fe_3O_4 nanoparticles without inert gas protection used as precursors of magnetic fluids. Journal of Magnetism and Magnetic Materials. 320(9): 1605-1614.

[28] Zhang, B., Xing J. M., and Liu H. Z. 2008. Synthesis and characterization of superparamagnetic poly(urea-formaldehyde) adsorbents and their use for adsorption of flavonoids from Glycyrrhiza uralensis Fisch. Adsorption. 14(1): 65-72.

[29] Nuthalapati, V., Ramalingam, C., Dasgupta, N., Ranjan, S., Varghese, L. R. and Mandal, S. K. 2014. Optimization of growth medium using a statistical approach for the production of plant gallic acid from a newly isolated Aspergillus tubingenesis NJA-1. Journal of Pure and Applied Microbiology. 8: 3313-3324.

[30] Marzuki, N. H. C., Huyop, F., Aboul-Enein, H. Y., Mahat, N. A. and Wahab, R. A. 2015. Modelling and optimization of Candida rugosa nanobioconjugates catalysed synthesis of methyl oleate by response surface methodology. Biotechnology & Biotechnological Equipment. 29(6): 1113-1127.

[31] Rahman, M. B. A., Chaibakhsh, N., Basri, M., Rahman, R. N. Z. R. A., Salleh, A. B. and Radzi, S. M. 2008. Modeling and optimization of lipase-catalyzed synthesis of dilauryl adipate ester by response surface methodology. Journal of Chemical Technology & Biotechnology. 83(11): 1534-1540.

[32] Singh, K. P., Gupta, S., Singh, A. K. and Sinha, S. 2010. Experimental design and response surface modeling for optimization of Rhodamine B removal from water by magnetic nanocomposite. Chemical Engineering Journal. 165(1): 151-160.
[33] Behera, S. K., Meena, H., Chakraborty, S. and Meikap, B. C. 2018. Application of response surface methodology (RSM) for optimization of leaching parameters for ash reduction from low-grade coal. International Journal of Mining Science and Technology. 28(4): 621-629.
[34] Shen, K. and Gondal M. 2017. Removal of hazardous Rhodamine dye from water by adsorption onto exhausted coffee ground. Journal of Saudi Chemical Society. 21: 120-127.
[35] Das, S., Dash S. K, and Parida K. M. 2018. Kinetics, isotherm, and thermodynamic study for ultrafast adsorption of azo dye by an efficient sorbent: ternary Mg/(Al + Fe) layered double hydroxides. ACS Omega. 3(3): 2532-2545.
[36] Cheng, Z., Zhang, L., Guo, X., Jiang, X., and Liu, R. 2015. Removal of Lissamine rhodamine B and acid orange 10 from aqueous solution using activated carbon/surfactant: process optimization, kinetics and equilibrium. Journal of the Taiwan Institute of Chemical Engineers. 47: 149-159.
[37] Dutta, S., Srivastava, S. K., Gupta, B., and Gupta, A. K. (2021). Hollow polyaniline microsphere/MnO_2/Fe_3O_4 nanocomposites in adsorptive removal of toxic dyes from contaminated water. ACS Applied Materials & Interfaces, 13(45): 54324-54338.
[38] Gecgel, U., Ozcan G., and Gurpinar G.C. 2012. Removal of methylene blue from aqueous solution by activated carbon prepared from pea shells (Pisum sativum). Journal of Chemistry. 26(2): 1-9.
[39] Golob, V. and Ojstrsek A. 2005. Removal of vat and disperse dyes from residual pad liquors. Dyes and Pigments. 64(1): 57-61.